Modeling reduction kinetics of iron ore/biochar composite pellets during inert heating and gas-based reduction

M.L. Ali[1*], S. Fong[1], Q. Fradet[1], N. Manolikakes[2], R.D. Putra[2], A. Schedl[2], U. Riedel[1]

[1] German Aerospace Center (DLR), Institute of Low-Carbon Industrial Processes,
Äußere Oybiner Straße 14/16, 02763 Zittau, Germany.
[2] DBFZ – Deutsches Biomasseforschungszentrum gemeinnützige GmbH,
Thermo-chemical Conversion Department, Torgauer Str. 116, 04347 Leipzig, Germany

Abstract: The steel industry is a major source of greenhouse gas emissions, motivating low-carbon ironmaking routes such as hydrogen direct reduction of iron ore. While this route avoids fossil carbon input, carbon is still required for downstream steelmaking. Iron ore composite pellets containing biochar can supply this in-situ carbon, offering higher fixed-carbon yield and greater thermal stability than raw biomass. In addition, part of the biochar contained in cold-bonded composite pellets can advantageously participate in the pre-reduction of the pellets through devolatilization and gasification prior to external gas reduction. Available modeling studies of direct reduction for composite pellets are scarce and typically restricted to isothermal conditions. In this work, a transient model is developed for single porous composite pellets subjected to experimental temperature profiles. Heating under inert gas followed by isothermal reduction under H_2, H_2/CO, and a biomass derived biogenic gas is simulated to predict pellet composition and mass loss evolution. The modeling framework accounts for moisture evaporation, devolatilization of biochar volatiles, gasification of biochar fixed carbon, and subsequent reduction of iron oxides by coupling intra-pellet transport with heterogeneous reaction kinetics. Model predictions show agreement with thermogravimetric measurements, demonstrating that the framework captures the reduction behavior of composite pellets under relevant experimental conditions.

1. INTRODUCTION

Direct reduction (DR) of iron ore is increasingly recognized as a key pathway for reducing greenhouse gas emissions in the steel industry, particularly through hydrogen-based direct reduction (H_2-DR), which eliminates the need for fossil carbon in the reduction stage [1]. However, carbon remains essential for downstream steelmaking, especially in electric arc furnaces (EAF), where it contributes to slag formation, energy efficiency, and process stability [2]. The absence of sufficient in-situ carbon in hydrogen-reduced iron therefore necessitates external carbon addition, which can negatively affect process efficiency and material consumption [3].

Iron ore composite pellets containing carbonaceous materials provide a potential solution by supplying internal carbon directly within the burden [4]. In particular, biomass-derived biochar offers a renewable alternative to fossil carbon, with favorable properties such as high fixed-carbon content, thermal stability, and reactivity [5]. During heating, biochar undergoes devolatilization, generating reducing gases (e.g., CO and H_2) within the pellet. These internally generated gases can initiate partial reduction prior to the introduction of external reducing gas, thereby influencing subsequent reduction behavior and pellet structure [6].

Despite these advantages, modeling studies of biochar-containing composite pellets remain limited. Existing approaches are often restricted to isothermal conditions or rely on lumped kinetic formulations that do not explicitly resolve the sequence of heating-stage processes, including moisture evaporation, devolatilization, and gasification [7-8]. As a result, the impact of heating history and internally generated gases on later gas-based reduction kinetics is not adequately captured.

In this work, a transient single-pellet modeling framework is developed to describe the coupled evolution of gas transport, gas-solid-phase reactions, and porosity in iron ore–biochar composite pellets. The model explicitly accounts for heating-stage transformations and their interaction with H_2, 50/50 H_2/CO, and biogenic gas reduction. Experimental thermogravimetric data are used to validate the model under non-isothermal heating followed by isothermal reduction. The objective is to provide a

* Corresponding author. E-mail: mohammed.ali@dlr.de, telephone: +49 358 35854-530.

mechanistic understanding of the role of biochar in composite pellets and its influence on reduction behavior under conditions relevant to hydrogen-based and biogenic gas ironmaking.

2. EXPERIMENTAL MATERIALS AND METHODS

Composite pellets were prepared from beechwood-derived biochar, iron oxide (≥ 96 wt.% Fe_2O_3), and a cement binder, with nominal mass fractions of 81.6 wt.% Fe_2O_3, ~14.9 wt.% biochar (as received), and ~3.6 wt.% cement. The biochar contained 88.1 wt.% fixed carbon and 4.2 wt.% ash (dry basis), with 10.1 wt.% moisture as received. Pellets with a mean radius of ~6.2 mm were produced by disc pelletization, cold-bonded, and dried under ambient airflow, resulting in ~60% porosity. Using a Linseis PT1600 thermogravimetric system, single pellets were heated at 30 K/min under N_2 (270 mL/min) up to 1173 K, then switched to one of three reducing gases (270 mL/min): (i) pure H_2, (ii) 50/50 vol.% H_2/CO, or (iii) biogenic gas (BG: 53% H_2, 33% CO, 10% CO_2, 3% CH_4, 1% N_2). Mass evolution was recorded continuously, with buoyancy effects corrected via blank runs.

3. MODELING

A one-dimensional transient porous pellet model was developed to describe gas transport, solid-phase reactions, and porosity evolution in biochar–iron ore composite pellets under inert heating and reduction by H_2, H_2/CO, and biogenic gas. The model builds on a previously developed porous pellet framework [9] and is extended here to explicitly describe composite pellet behavior. Gas-phase species transport is described by a diffusion–advection mass balance including evaporation rate, reaction source terms and porosity variation. Solid-phase species evolution is governed by reaction rates coupled with porosity changes, while porosity is determined from the net solid-phase source terms. Moisture evaporation is included as a phase-change process between solid and gas phases. The governing equations include gas-phase species balance (Eq. 1), solid-phase species balance (Eq. 2), porosity evolution (Eq. 3).

$$\frac{\partial C_i}{\partial \mathrm{t}} = \frac{1}{\varepsilon}\frac{1}{r^2}\frac{\partial}{\partial \mathrm{r}}\left(r^2 D^{\mathrm{eff}}\frac{\partial C_i}{\partial \mathrm{r}}\right) - \frac{1}{\varepsilon}\frac{1}{r^2}\frac{\partial}{\partial \mathrm{r}}(r^2 u C_i) + \frac{1}{\varepsilon}\dot{s}_i - \frac{C_i}{\varepsilon}\frac{\partial \varepsilon}{\partial \mathrm{t}},\ i \in \text{ gas species}, \tag{1}$$

$$\frac{\partial X_j}{\partial t} = \frac{1}{(1-\varepsilon)}\frac{M_j}{\rho_j}\dot{s}_j + \frac{X_j}{(1-\varepsilon)}\frac{\partial \varepsilon}{\partial t},\ j \in \text{ solid species}. \tag{2}$$

$$\frac{\partial \varepsilon}{\partial t} = -\sum_j \frac{M_j}{\rho_j}\dot{s}_j,\ j \in \text{ solid species}. \tag{3}$$

Here, C_i is gas concentration, ε porosity, u gas velocity, D_i^{eff} effective diffusivity, X_j solid-phase fraction, and ρ_j solid-phase density. The source terms $\dot{s}_{i/j}$ represent heterogeneous reaction contribution [9], extended here to account for moisture evaporation. The evaporation rate r_{evap} is modeled as a first-order mass-transfer expression (Eq. 4), where K_{int} is the internal mass-transfer coefficient and C_{eq} and $C_{\mathrm{H_2O}}$ are the equilibrium and local water vapor concentrations, respectively.

$$r_{\mathrm{evap}}(r,t) = K_{\mathrm{int}}\left[C_{\mathrm{eq}}(T,P) - C_{\mathrm{H_2O}}(r,t)\right]. \tag{4}$$

The kinetic scheme includes iron oxide reduction by H_2 and CO, as well as carburization, carbon deposition reactions, and related gas-phase reactions as described in our previous work [10,11], since biochar-derived gases generated during heating create an internally reducing atmosphere. Heating-stage reactions are additionally included: devolatilization of biochar (Eq. 5) with stoichiometric coefficients adopted from Wang et al. [12], and gasification of fixed carbon via steam (Eq. 6) and CO_2 (Eq. 7).

$$\text{Volatiles}_{(s)} \rightarrow 0.56\ H_{2(g)} + 0.23\ H_2O_{(g)} + 0.06\ CO_{(g)} + 0.11\ CO_{2(g)} + 0.04\ CH_{4(g)} \tag{5}$$

$$C_{f(s)} + H_2O_{(g)} \rightarrow CO_{(g)} + H_{2(g)} \tag{6}$$

$$C_{f(s)} + CO_{2(g)} \rightarrow 2\ CO_{(g)} \tag{7}$$

4. RESULTS & DISCUSSIONS

Fig. 1 presents the experimentally measured and model-predicted normalized mass evolution $m(t)/m_0$ for iron ore–biochar composite pellet heated to 1173 K under N_2 and subsequently reduced under H_2, 50/50 H_2/CO, and BG. Panel (a) depicts all the three experimental cases together, whereas (b)–(d) compare model predictions with experimental data individually, with inset pie charts showing the model-predicted solid-phase compositions at gas-switch onset (t ~49 min) and end of reduction (t ~80 min).

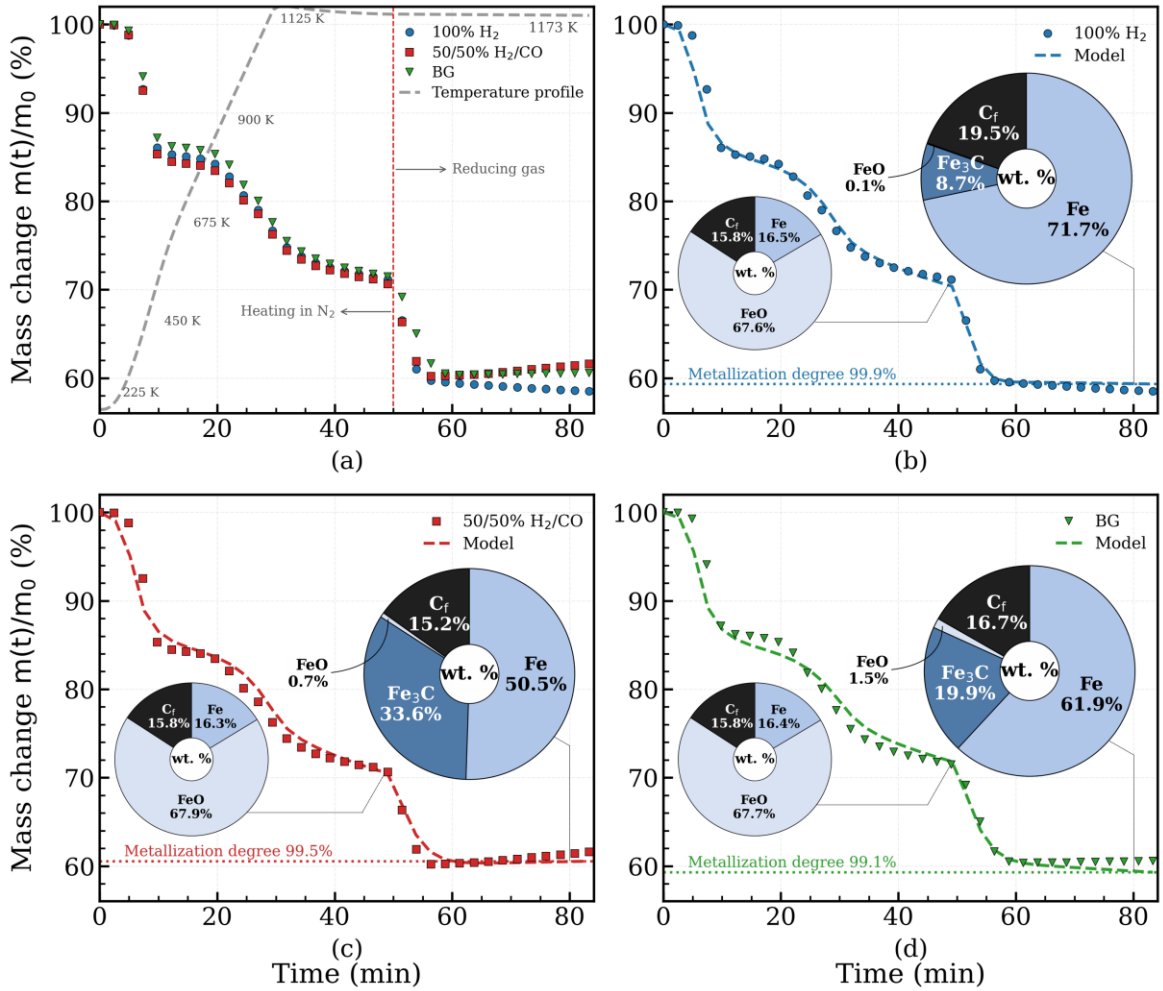


Figure 1. Normalized mass evolution $m(t)/m_0$ of composite pellets during inert heating in N_2 to 1173 K (left of red vertical dashed line) and subsequent isothermal reduction (right of red vertical dashed line). (a) Overlay of all three gas cases with temperature profile; (b)-(d) individual model and experiment comparisons for H_2, 50/50 H_2/CO, and BG, with model-predicted solid-phase compositions at gas-switch onset and end of reduction. Dotted horizontal lines indicate modelled final metallization degree.

The mass evolution curves for all three cases during the heating with N_2 (time < 50 min) are virtually identical, confirming the reproducibility of the pellet preparation and the consistency of the pre-reduction thermochemical pathway across all three experiments. During the heating stage, the pellet loses approximately 30% of its initial mass, reflecting three sequential processes. An initial sharp drop between 0 and ~10 min corresponds to evaporation of free moisture and release of volatile matter from the biochar. A region of slow, decelerating mass loss between approximately 10 and 20 min represents a kinetically enforced interval in which all volatile species are exhausted yet the lignocellulosic char gasification with CO_2 (Eq. 7) does not occur as the corresponding temperature at that time is below 1000 K [13]. A second, more prominent mass-loss region, from ~20 min until the gas switching, marks the activation of the internal carbothermal reduction of iron oxides generating CO_2, which gasifies the char

(Eq. 7) to produce CO, driving further oxide reduction in a self-sustaining loop despite the external N_2 atmosphere.

Upon introduction of the reducing gas at t ≈ 50 min, all three cases undergo rapid mass loss, with curves converging toward a final normalized mass of approximately 59–62%. The sharp reduction onset is consistent with fast reaction of the external reductant with pre-formed FeO accumulated during the N_2 stage. The high initial porosity (~60%), further increasing to ~82% upon full reduction as predicted by the model, ensures that gas transport remains uninhibited throughout, facilitating rapid and near-complete reduction regardless of gas composition. The near-identical final mass loss across all three gas compositions suggests that at 1173 K, all three reducing gases provide sufficient driving force for near-complete iron oxide reduction, such that the final mass loss is insensitive to gas composition, a conclusion that, however, conceals fundamentally different solid-phase outcomes as revealed by the model.

Model predictions (dashed lines in panels b–d) show good agreement with experimental data throughout both the heating and reduction stages for all three gas compositions. The model-predicted solid compositions at gas-switch onset are virtually identical across all cases: ~16.4 wt.% Fe, ~67.7 wt.% FeO, and ~15.8 wt.% C_f, with negligible Fe_2O_3 and Fe_3O_4 remaining, corresponding to a metallization degree of ~34.1% achieved purely under inert N_2, highlighting the significant self-reduction potential of composite biochar pellets prior to any external reducing gas. Despite similar final mass loss, solid compositions differ markedly: metallization reaches 99.9%, 99.5%, and 99.1% while Fe_3C content varies strongly; 8.6, 33.6, and 19.9 wt.% for H_2, H_2/CO, and BG respectively. This reveals that mass loss alone is an insufficient discriminator between gas compositions. Fe_3C formation is highly sensitive to the CO_2/H_2O content of the reducing gas, as the higher carburization in H_2/CO relative to BG is attributed to the absence of CO_2 and H_2O, which otherwise inhibit cementite formation [11]. From a steelmaking perspective, this distinction is critical: Fe_3C is a desirable EAF feedstock carrying ~6.7 wt.% carbon, reducing the need for external carbon injection. BG thus serves a dual role: partially replacing scarce H_2 while delivering renewable carbon as Fe_3C, complementing the in-situ carbon from the embedded biochar. The remaining C_f (15.2–19.3 wt.%) further contributes to the carbon inventory for downstream steelmaking, supporting a pathway toward fossil-free, carbon-neutral ironmaking.

These results establish composite biochar pellets as a viable feedstock for fossil-free ironmaking, with biogenic reducing gases offering a practical H_2-lean pathway that simultaneously enriches the product in renewable carbon. The validated single-pellet framework provides a foundation for upscaling to reactor-level modeling of fixed-bed direct reduction processes.

Acknowledgements: We acknowledge funding by the European Union and by tax revenues on the basis of the budget adopted by the Saxon State Parliament (European Regional Development Fund (EFRE) project “BioFe - Biomassenutzung in der Eisenerzeugung unter wirtschaftlichen und CO2-mindernden Randbedingungen”).

REFERENCES

[1] K. Rechberger, A. Spanlang, A. Sasiain Conde, H. Wolfmeir and C. Harris: steel research international, 19 (2020), 2000110.
[2] T. Echterhof: Metals, 11 (2021), 222.
[3] L. Kieush and J. Schenk: steel research international, 96 (2025), 2400235.
[4] Y. Matsui, M. Sawayama, A. Kasai, Y. Yamagata and F. Noma: ISIJ International, 43 (2003), 1904–1912.
[5] E. Mousa, C. Wang, J. Riesbeck and M. Larsson: Renewable and Sustainable Energy Reviews, 65 (2016), 1247–1266.
[6] J. Yang, T. Mori and M. Kuwabara: ISIJ International, 47 (2007), 1394–1400.
[7] G. Wang, J. Zhang, G. Zhang, H. Wang and Di Zhao: ISIJ International, 57 (2017), 1374–1383.
[8] J. Shi, E. Donskoi, D. McElwain and L. J. Wibberley: Mathematical and Computer Modelling, 42 (2005), 45–60.
[9] Q. Fradet, M. L. Ali and U. Riedel: steel research international, 93 (2022), 2200042.
[10] M. L. Ali, Q. Fradet and U. Riedel: steel research international, 93 (2022), 2200043.
[11] S. Fong, M. L. Ali, S. Mehlhose, Q. Fradet, R. Putra, A. Schedl, U. Riedel: Particuology, 114 (2026), 236-255.
[12] T. Wang, O. Mirgaux and F. Patisson: Chemical Engineering Science, 319 (2026), 122319.
[13] C. Di Blasi: Progress in Energy and Combustion Science, 35 (2009), 121–140.